
This is an electronic reprint of the original article.
This reprint may differ from the original in pagination and typographic detail.

Kaur, P.; Park, Y.; Imteaz, M. A.; Sillanpaa, M.

Synthesis of non-active electrode (TiO₂/GO/Ag) for the photo-electro-Fenton oxidation of micropollutants in wastewater

Published in:
International Journal of Environmental Science and Technology

DOI:
[10.1007/s13762-022-04065-3](https://doi.org/10.1007/s13762-022-04065-3)

Published: 01/01/2023

Document Version
Publisher's PDF, also known as Version of record

Published under the following license:
CC BY

Please cite the original version:
Kaur, P., Park, Y., Imteaz, M. A., & Sillanpaa, M. (2023). Synthesis of non-active electrode (TiO₂/GO/Ag) for the photo-electro-Fenton oxidation of micropollutants in wastewater. *International Journal of Environmental Science and Technology*, 20(1), 639–652. <https://doi.org/10.1007/s13762-022-04065-3>

This material is protected by copyright and other intellectual property rights, and duplication or sale of all or part of any of the repository collections is not permitted, except that material may be duplicated by you for your research use or educational purposes in electronic or print form. You must obtain permission for any other use. Electronic or print copies may not be offered, whether for sale or otherwise to anyone who is not an authorised user.



Synthesis of non-active electrode (TiO₂/GO/Ag) for the photo-electro-Fenton oxidation of micropollutants in wastewater

P. Kaur^{1,2} · Y. Park^{2,3} · M. A. Imteaz⁴ · M. Sillanpaa^{5,6,7,8}

Received: 13 November 2020 / Revised: 29 December 2021 / Accepted: 2 March 2022 / Published online: 26 March 2022
© The Author(s) 2022

Abstract

Heterogeneous photo-electro-Fenton oxidation (hPEF) is known to be a robust technique, which can be employed for promoting organic degradation. This paper describes an environmentally friendly approach with the combination of photocatalysis and electrocatalysis in less acidic pH, aiming to achieve faster mineralization of a pharmaceutical micropollutant without adding any external oxidants. TiO₂/GO/loaded Ag non-active electrodes are synthesized for the degradation of bupropion hydrochloride (antidepressant drug). The present work also seeks the parametric modeling and optimization of hPEF process parameters by using R programming. Nonlinear kinetic modeling was performed for the determination of kinetic parameters. The role of selected process parameters on the mineralization of bupropion was also explained in detail. The OH• and O₂•⁻ showed their active participation in the degradation process, while Ag and UV-C played an active role in the disinfection of treated wastewater.

Keywords Heterogeneous photo-electro-Fenton · TiO₂/GO/Ag-loaded electrodes · R programming · Response surface model · Micropollutants

Introduction

The issue of micropollutants is as of now probably the most sizzling topic in environmental engineering, because of their ubiquitous presence in natural water bodies (Aliofkhaezai 2014). One of the most conspicuous transport pathways of micropollutants is urban wastewater treatment plants since these wastewater treatment plants are usually not equipped with the best possible treatment sequences to remove of

micropollutants from wastewater (An et al. 2019; Cheng et al. 2014). Hence, high amounts of micropollutants are diluted in the receiving wastewater and led to treatment.

Advanced oxidation processes (AOPs) are efficient to treat an extensive range of industrial wastewater and an environment-affable green technology (Chèvre 2014). Among all the AOPs, photo-Fenton (PF) and electro-Fenton (EF) have been demonstrated as promising treatment methods for micropollutants along with other pollutants that have received great attention for water remediation because of

Editorial responsibility: iskender AKKURT.

✉ P. Kaur
parminder.kaur@aalto.fi

¹ Department of Chemical and Metallurgical Engineering, Aalto University, 00076 Espoo, Finland

² Department of Separation Science, LUT University, 50130 Mikkeli, Finland

³ Department of Environmental Engineering, Seoul National University of Science and Technology, Seoul 01811, South Korea

⁴ Department of Civil & Construction Engineering, Swinburne University of Technology, Melbourne, Australia

⁵ Department of Chemical Engineering, School of Mining, Metallurgy and Chemical Engineering, University of Johannesburg, P. O. Box 17011, Doornfontein 2028, South Africa

⁶ Department of Civil Engineering, University Centre for Research & Development, Chandigarh University, Mohali, Punjab 140413, India

⁷ Chemistry Department, College of Science, King Saud University, 11451 Riyadh, Saudi Arabia

⁸ Zhejiang Rongsheng Environmental Protection Paper Co. LTD, NO.588 East Zhennan Road, Pinghu Economic Development Zone, 314213 Zhejiang, P.R. China



being economical, efficient, and having a simple configuration (Farshchi et al. 2019). Nowadays, the synergic effect of photo- and electrocatalytic oxidation of environmental pollutants has attained a great pace. It has been reported that nanostructured materials and modified electrodes materials provide high overall pollutant removal efficiency. (Fatta-Kassinos et al. 2011).

Titanium dioxide (TiO_2) is broadly engaged with photo(electro)catalysis. It is ascribable to its vast range of properties and could be used in different morphologies and energy positions (Feng et al. 2006; Fox et al. 2012; Gao et al. 2008; Hu et al. 2010). It is also reported that the modified TiO_2 as a material or in the form of electrodes provides a magnificent electronic shift of photogenerated charge carriers and reduces the recombination rate of electron/hole pair (Jia et al. 2016). Therefore, the major goal of the present research was to synthesize TiO_2 non-active modified electrodes to eliminate the hindrances for a realistic approach to heterogeneous photo-electrocatalysis (hPEF). The major hindrance for the use of hPEF in water treatment is a very narrow pH range to achieve a maximum efficiency and leaching out of electrocatalytic materials into the treated wastewater and contributions to additional water pollution, which cannot be retained in the process. To overcome the bottlenecks of the hPEF process, development of a non-active electrocatalyst is necessary, which will inactively participate in the reaction without leaching of catalytic material into the water, and a Fenton reagent is required to widen the pH range of Fenton reaction. Therefore, in the present study, TiO_2 -graphene oxide (GO)-loaded silver nanoparticles (Ag) non-active electrodes were fabricated and $\alpha\text{-Fe}_2\text{O}_3/\alpha\text{-FeOOH}$ was used as Fenton reagent. Bupropion was used as a model compound, and its degradation with a non-active mixed metal electrode ($\text{TiO}_2\text{-GO-Ag}$) by hPEF treatment method has not been reported in the literature.

The most important aspect of the successful degradation of organics in wastewater has been parametric optimization of process. The traditional process optimization approach does not show the collective effect of all the independent variables over the responses. Furthermore, a traditional process optimization approach is rather time-consuming and requires lots of experiments to be performed. The statistical experimental design overcomes these restrictions of the traditional process optimization approaches. Response surface methodology is an effective optimization tool for the simultaneous optimization of process parameters with fewer experimental trials. Several commercial optimizations software tools provide optimization process approaches; however, R is open-source software, which allows the execution of various statistical techniques by using different packages. It offers a broad range of statistical and graphical techniques with more updated packages. R software packages are very sensitive and useful in the optimization process through the

validation approach (Kumar et al. 2008). So, for the present study, R open-source software by R-Commander (Rcmdr) package with RcmdrPlugin. DoE plugin has been used for parametric modeling of hPEF process. To the best of authors' knowledge, there are no reports on the use of the statistical design of R package for simultaneously optimization of hPEF process parameters. Furthermore, the degradation mechanism and disinfection study for the treatment of bupropion wastewater by the hPEF treatment has been performed. The change in the rate of reaction or reaction kinetics has also been studied.

Materials and methods

TiO₂/GO/Ag-loaded nanostructured electrode fabrication

A seamless perforated Ti tube (Global Engineers, India) with a 165-cm^2 area was used as a base material for electrode fabrication. Perforated Ti tube was furnished using sandpaper and then cleaned with 70% isopropanol and ultrapure water. Graphene oxide was fabricated over the surface of TiO_2 -perforated seamless tube by the anodization method. Ultrasound waves (Branson 2510 sonicator) were used for the mechanical itching of TiO_2 tube by using (acetone)1:(water)10 for 60 min. Furthermore, (HF)1:(HNO_3)4:(H_2O)10 was used for the chemical engraving of Ti tube for 10 to 20 s. Anodization was performed with TiO_2 seamless perforated tube (3 cm) as a positive electrode and copper tube (3 cm) as a negative electrode. The distance maintained between the electrodes was 1 cm in 5% HF electrolyte at 20 V (Astral-PS3005 power supply (0–30v)) for 2 h. The fresh anodized electrode was calcinated in the muffle furnace at $500\text{ }^\circ\text{C}$ (Nabertherm muffle furnace L 5/11) for 3 h. Graphene oxide (GO; 10 ml L^{-1}) was deposited on the surface of TiO_2 nanostructured electrode by anodization at 15 V for 10 min and then calcinated at $350\text{ }^\circ\text{C}$ for 2 h. Furthermore, GO- TiO_2 electrode was taken as a cathode and steel electrode as an anode. Electro-deposition was performed ($100\text{ ml L}^{-1}\text{AgNO}_3$) for 10 min at 15 V for the coating of Ag. Annealing was carried out at $200\text{ }^\circ\text{C}$ for 2 h. To confirm the fabrication electrodes, characterization was performed. The crystal structure was examined using an X-ray diffractometer (XRD) of the Empyrean series 2 PANalytical X-ray with Co-anode (40 kW, 30 mA). A high dynamic range pixel 3D detector with a monochromator was used for the detection of diffracted X-rays. Raman spectroscopy (HORIBA Jobin Yvon LabRAM HR, model number: HR800VIS-UVL-2005-057, 514.53 nm) was performed for the detailed information about the chemical structure and molecular interaction properties of the electrode. The surface topography and composition of the fabricated electrode

were studied by SEM (Hitachi S-4800). Energy-dispersive spectrometry (EDS) is an analytical technique used for the elemental analysis or chemical characterization of the electrodes.

Pharmaceutical drug

Bupropion hydrochloride of the aminoketone class (anti-depressant) was purchased from Sigma–Aldrich (99.9% purity). Its structure closely resembles with diethylpropion and is correlated with phenylethylamines. The molecular formula is $C_{13}H_{18}ClNO \cdot HCl$. Bupropion hydrochloride powder is white, crystalline, and highly soluble in water. Simulated pharmaceutical wastewater was prepared by dissolving 5 mgL^{-1} (Mettler Toledo micro weighing balance) of bupropion hydrochloride. Antidepressants are present in the wastewater in very small amounts but highly toxic for the environment (Lawson 2014).

Experimental setup

A batch reactor was designed at a laboratory scale for the treatment of simulated pharmaceutical wastewater by hPEF process with a working volume of 1 L, and sintered bubblers were used for injecting air into the electrochemical reactor. The reactor was placed in the center of UV chamber with two UV-C, 8 W lamps as shown in SI-1. A seamless perforated $TiO_2/GO/Ag$ -loaded nanostructured electrode as anode and cathode was placed inside the glass reactor. The current or voltage was controlled using an astral-PS3005 power supply (0–30 V). The distance between the anode and cathode was maintained at one cm. All the experiments were performed in a laboratory with excellent exhaustion.

Experimental design, data analysis, and modeling by R

R is a language and environment for statistical computing and graphics. It provides a wide variety of statistical computations such as linear and nonlinear modeling and classical statistical tests. It is easily extensible through functions and extensions, and the R community has for its active contributions in terms of packages (Li et al. 2007). R by Rcmdr (design) package from CRAN was used for the designing of the hPEF experiments. The response surface model (RSM) was used for the modeling of hPEF process. pH, time (min), voltage (V), and $\alpha\text{-Fe}_2\text{O}_3/\alpha\text{-FeOOH}$ dose (mM) were taken as four independent variables for the hPEF process for the degradation of simulated pharmaceutical wastewater with respect to the % TOC removal (%T), % mineralization (%M), and energy efficiency (EC). Four levels were selected for each independent factor, to investigate the interaction of these independent factors and its effect over the response.

Experiments were performed to prove the accuracy using the levels/ranges of each selected factor. The response variables were fitted by a sufficient model and able to describe the interaction between the selected responses and the independent variables using the regression method. In RSM, the relationship between the responses (R) and the independent variables (Iv) was assumed to be a nonlinear Eq. (1), where f is a nonlinear function and ∂ is the random effect of experimental error.

$$R = f(Iv) + \partial \quad (1)$$

The RSM requires that it must provide data that will allow estimation of the coefficients of the model. Among the response surface designs, the most popular one is the central composite design (CCD). This design allows for the sequential augmentation, first allows one block for the fitting of first-order model and then adds more blocks if the second-order model fitting is required. There are two types of blocks in CCD, i.e., cube blocks (two-level factorial + center points) and star blocks (axis points + center points). The levels of the factors are at positions ± 1 and center points at $(0, 0, \dots, 0)$. The design points in the star blocks are at the position of $\pm \alpha$ along each coordinate axis. The value of α and choices of replications of the design points and center points are often selected based on the consideration of rotatability and orthogonality of blocks (Lin et al. 2019).

The desirability package from CRAN was used for the optimization of responses. The synchronized optimization is a collective form of overall desirability function approach and maximizes desirability within a cuboidal region bounded by the value of the axial points. This optimization technique can handle discontinuous or non-smooth functions that are commonly produced by desirability functions. The desirability function within a cuboidal region changes each response to congruous desirability (α_i) value between 0 and 1 as expressed in Eq. (2), where R_i is the response value, $R_{i\text{-min}}$ and $R_{i\text{-max}}$ are the minimum and maximum admissible values of responses i , respectively, and π are weights and a positive constant. These are used to determine the scale of desirability. The combination of all desirability functions provides composite desirability function as shown in Eq. (3), where $0 \leq \alpha \leq 1$, and Ω is the number of responses (Lin et al. 2019).

$$\alpha_i = \begin{cases} 0 & \left[\frac{R_i - R_{i\text{-min}}}{R_{i\text{-max}} - R_{i\text{-min}}} \right]^\pi \\ 1 & \end{cases} \quad (2)$$

$$\alpha = (\alpha_1 \times \alpha_2 \dots \alpha_n)^{\frac{1}{\Omega}} \quad (3)$$

The samples were analyzed for the selected responses, i.e., % T, % M, and EC. % T was determined by using the Hach cuvette test LCK 380 (DR 3900 spectrophotometer).



% T was calculated by using Eq. (4), where T_1 = initial TOC and T_2 = final TOC. The % M was analyzed using a double-beam UV–visible spectrophotometer (HACH, DR 5000, USA). The λ_{max} for bupropion was 254 nm, and Eq. (5) was used to measure % M , where A_1 = initial absorbance and A_2 = final absorbance. EC response was calculated using Eq. (6), where i = current (A), V = voltage (v), t = time (h), and φ = reactor working volume (l).

$$\%T = \left[\frac{T_1 - T_2}{T_1} \right] \times 100 \quad (4)$$

$$\%M = \left[\frac{A_1 - A_2}{A_1} \right] \times 100 \quad (5)$$

$$EC = \left[\frac{Vti}{\varphi} \right] \text{ Wh} \quad (6)$$

Degradation mechanism and disinfection study

UV spectrophotometric, Fourier transform infrared spectroscopy (FTIR), electron paramagnetic resonance (EPR) with spin trapping, and gas chromatography–mass spectrometry (GC–MS) were performed to predict the plausible degradation mechanism of bupropion by hPEF treatment method. Treated (by hPEF) and untreated simulated pharmaceutical wastewater was analyzed under the UV range of spectrophotometer to observe the reduction of peaks of bupropion before and after treatment. FTIR (Vertex 70, Bruker) was used to observe the stretching and breaking of bupropion molecule bonds and the formation of new bonds after hPEF treatment. EPR (EPRA-9300/CMS 8400) was used to observe the generation of radicals during the hPEF treatment process. The compounds identified by GC–MS analysis of the treated simulated pharmaceutical wastewater by hPEF were analyzed through a comparison of original simulated pharmaceutical wastewater. The sample for GC–MS analysis was prepared by the liquid–liquid extraction method using dichloromethane. GC–MS (Agilent Technologies) with ZB drug column (30 m \times 0.25 μm internal diameter, 0.25 μm thickness) was used for GC–MS analysis. Injector temperature was 250 $^\circ\text{C}$ at splitless injector mode. Carrier gas for GC was helium with a flow rate of 0.6 ml/min. The temperatures of the inlet line and ion sources were 250 $^\circ\text{C}$ and 260 $^\circ\text{C}$, respectively. The total time for the GC–MS analysis run was 30 min.

To study the disinfection activity standard, colonies forming units (CFU) method was used (APHA manual). The comparative disinfection properties of the hPEF process in the presence of Ag, UV-C, and Ag + UV-C were observed. DH $\alpha 1$ cells of *Escherichia coli* (*E. coli*) were

cultivated at 37 $^\circ\text{C}$, maintained on LB plates (Luria–Bertani agar), and then, at exponential phase, harvested by centrifugation. Harvested *E. coli* cells were inoculated in the sterile 0.9% NaCl solution. Furthermore, DH $\alpha 1$ strain of *Escherichia coli* (*E. coli*) was used for the disinfection study of synthetic pharmaceutical wastewater by hPEF treatment process.

Results and discussion

Electrode characterization

The electrochemical anodization method was used for the synthesis of TiO₂/GO/Ag-loaded electrodes. The characterization of the electrodes was performed by XRD, Raman spectroscopy, and SEM–EDS. TiO₂ phase was confirmed by XRD, and Fig. 1a shows the TiO₂ anatase diffraction peaks at 29.45 $^\circ$, 31.93 $^\circ$, 48.2 $^\circ$, 63.4 $^\circ$, 74.3 $^\circ$, and 82.07 $^\circ$ planes (JCPDS CARD No. 21-1272). Anatase phase provides a better photocatalytic activity by exhibiting more charge carriers as compared to the rutile phase by avoiding the combination of charge carriers (Lucas and Peres 2009). The XRD analysis of TiO₂/GO/Ag-loaded fabricated electrode showed peaks at 29.44 $^\circ$, 44.68 $^\circ$, 62.22 $^\circ$, and 74.52 $^\circ$ (JCPDS No. 65-2871). It provides the information regarding the possibility of Ag. It was observed that a few peaks in the XRD pattern were overlapped. The loading of GO layer over TiO₂ was confirmed by a peak at 40.2 $^\circ$. The presence of Ag nanoparticles was not ensured by the XRD analysis.

To ensure the presence of Ag nanoparticles over the carbon layer, Raman spectroscopy was performed. The presence of anatase TiO₂ was confirmed by the presence of peaks at ~ 142 (E_g), ~ 396 (B_{1g}), and 514 (A_{1g}) (Metcalf et al. 2010) as shown in Fig. 1b. The presence of D and G peaks at ~ 1232 cm^{-1} and ~ 1403 cm^{-1} , respectively, confirmed the presence of graphene layer. The D and G peaks are representative peaks of carbon, indicating the presence of carbon with impurities, and E_{2g} carbon mode confirmed sp²-configured two-dimensional hexagonal layer of carbon (Mondal et al. 2018). Raman analysis also confirmed the possibility of Ag nanoparticle deposition over the electrode.

To confirm the presence of silver nanoparticles over the electrodes, the morphological characterization of the fabricated TiO₂/GO/Ag-loaded electrode was carried out by SEM–EDS. Soft puffed graphene layer was observed clearly over the TiO₂ substrate as shown in Fig. 1c (1). Furthermore, the electrodeposition of Ag nanoparticles was observed as bright circular stable nanoparticles over the TiO₂/GO surface (Fig. 1c (2)). The existence of TiO₂, GO, and Ag nanoparticles was confirmed by the EDS elemental analysis as presented in Table SI-1.

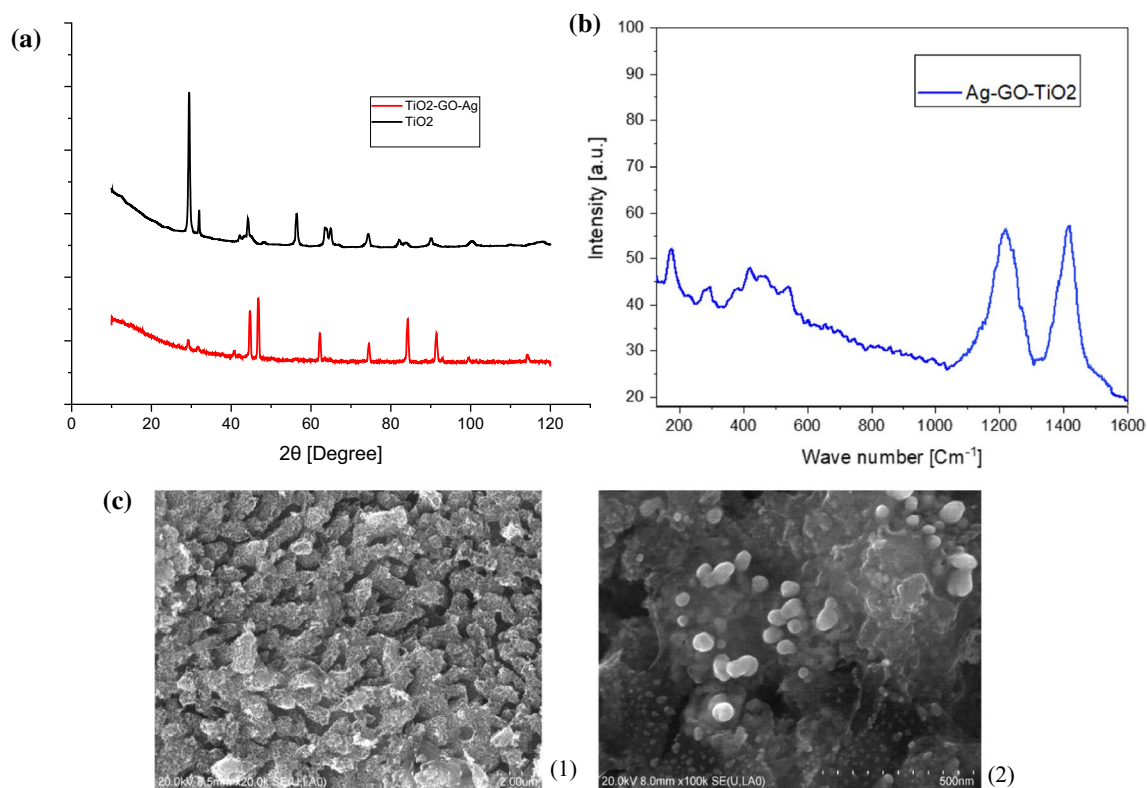


Fig. 1 a XRD patterns of TiO_2 and Ag-loaded GO/ TiO_2 electrodes. b Raman spectroscopy of Ag-loaded GO/ TiO_2 electrodes

Design of experiments, analysis, and optimization with R

Using the Rcmdr (design) package and the response surface central composite design (fractional factorial two-level design), the experiments for hPEF treatment process were designed. In the full factorial design, four independent variables were manipulated and all combinations of the levels of each independent variable were included. There were three selected response variables, namely % T , % M , and EC, and four coded predictors, namely X_1 , X_2 , X_3 , and X_4 . The ranges of the selected independent variables were selected based on preliminary experiments as shown in Table SI-2. The total number of 29 experiments was designed with the five central points. The experiments in the laboratory were conducted according to the matrix as shown in Table 1. The ‘rsm’ function was used for parametric modeling. The response surface portion was specified by the pure quadratic function because the model formula for ‘rsm’ was PQ (pure quadratic).

The interaction between the independent factors and dependent factors was estimated by significant model terms in the form of significant codes (0 ‘***’: highly significant, 0.001 ‘**’: significant, 0.01 ‘*’: comparatively significant) using response surface model as shown in Table 2. The obtained values of different R^2 for % T , % M , and EC were 0.967, 0.968, and 0.951, respectively. The significance

model terms were identified by processing ANOVA and the lack-of-fit F values which were insignificant: 0.763, 0.867, and 3.206 for % T , % M , and EC, respectively. P value less than 0.05 shows the significance of model terms with 95% confidence level as shown in Table 3.

To analyze the impact of individual independent factors (variables) such as pH, time (min), voltage (V), and $\alpha\text{-Fe}_2\text{O}_3/\alpha\text{-FeOOH}$ (mM) (Fe dose) on the dependent factors (response), i.e., % T removal (X_1), % M (X_2), and EC (Wh) (X_3), 3D response surface plots (Fig. 3, SI-2, and SI-3) were used. Figure 2a depicts that the % T efficiency was poor in a highly acidic medium (pH 3); at pH > 3, % T was begun to increase up to pH value of ≈ 7 . Subsequently, in the alkaline condition (pH > 8), the % T removal efficiency was abruptly decreased (Navalon et al. 2010). It was observed that voltage had very less impact on the % T at nearly neutral pH range but % T was extremely reduced at a low applied voltage (2 V). The interactive effect of Fe dose and time is shown in Fig SI-2a. As the hPEF reaction time was increased, the % T efficiency increases. But, as compared to higher Fe dose $\approx > 0.5$ mM, the enhancement in % T value with time was more protruding for lower values of Fe dose (0.2–0.5 mM). In Fig SI-2b, % T was found to increase with the increase in pH up to neutral with the increase in Fe dose to 0.5 mM. The highest % T was attained in the pH range of 5 to 7 for time ≈ 16 to 20 min at the lower range of Fe dose ≈ 0.3 to 0.6.

Table 1 Experimental matrix using the central composite design by R

Block	Runs	pH (X_1)	Time (min) (X_2)	Voltage (v) (X_3)	α -Fe ₂ O ₃ / α -FeOOH dose (mM) (X_4)	TOC Removal (% T)	Mineralization (% M)	Energy consumed (EC)
1	1	9	10	5	0.8	24.14	31.14	0.875
1	2	5	10	5	0.4	61.31	71.31	0.621667
1	3	9	20	3	0.8	3.63	13.63	1.47
1	4	5	20	5	0.4	79.01	90.01	1.55
1	5	9	10	3	0.4	20.66	25.66	0.725
1	6	7	15	4	0.6	69.61	79.61	1.05
1	7	9	20	3	0.4	35.94	45.94	1.65
1	8	7	15	4	0.6	52.1	62.1	1.05
1	9	5	20	3	0.8	32.76	42.76	0.85
1	10	9	20	5	0.8	21.51	31.51	1.85
1	11	5	20	5	0.8	39.1	29.1	1.1
1	12	7	15	4	0.6	69.32	79.32	1.05
1	13	7	15	4	0.2	87.66	97.66	1.35
1	14	7	15	4	0.6	68.01	78.01	1.05
1	15	7	25	4	0.6	66.39	76.39	1.95
2	16	9	10	3	0.8	20.8	26.8	0.425
2	17	9	10	5	0.4	15.45	25.45	0.55
2	18	11	15	4	0.6	3.22	9.22	1.45
2	19	5	10	3	0.8	55.43	65.43	0.325
2	20	9	20	5	0.4	48.23	58.23	1.95
2	21	7	15	4	0.6	68.71	77.71	1.05
2	22	7	5	4	0.6	55.28	60.28	0.11
2	23	5	10	5	0.8	40.55	50.55	0.31
2	24	5	20	3	0.4	89.89	99.89	1.35
2	25	5	10	3	0.4	77.99	87.99	0.125
2	26	7	15	2	0.6	20.29	32.29	0.725
2	27	7	15	4	0.6	66.5	75.5	1.05

Figure 2b illustrates the interactive impact of voltage and pH on mineralization efficiency (% M). The considerable advancement in % M was observed when the pH of the electrochemical system was increased from 2 to ≈ 7 , for all the voltage values. Nevertheless, an increase in pH up to ≈ 10 exhibited no change in % M . Comparably, over a whole range of Fe dose, maximum % M was achieved at pH ≈ 5 –7 (Fig SI-2c). The impact of voltage over the % M and % T followed a similar trend. Hence, the highest % M was observed in the pH range 5–6 at applied voltage ≈ 3.5 v. With the increase in time from 10 to 30 min, % M followed a linear trend for all Fe doses values from 0.2 to 0.6 mM (Fig SI-2d). In the present study, the finest results for % T and % M were achieved at the pH value of 5.8, which was not highly acidic. The oxidants involved in the destruction of pollutants were generated in the bulk solution or anode surface. Nevertheless, the generation of oxidants or efficiency in terms of % T and % M removal was comparatively low in highly acidic and very low in highly basic pH range. Figure 2c depicts that as

the voltage of the hPEF system increases with the increase in time, there was a sharp increase in the EC. The Fe dose and pH had no effect on the EC during the treatment process.

The interactive behavior of the independent parameters concerning the responses depicts that the pH range 5 to 7 promoted a bit higher performance in % T and % M . The catalytic mineralization process of hPEF voltage plays a powerful role. The movement of charge carriers in between TiO₂, GO, and Ag and the improvement in the charge separation is directly related to the applied voltage (Nidheesh et al. 2017). The % T and % M results concerning applied voltages > 3 were higher than the flat band potential of TiO₂. The applied voltage > 3 was enough for the complete band bending to promote the separation of the photogenerated charge carriers (Paramasivam et al. 2012). Therefore, a greater bias potential was circumvented side reactions during the hPEF wastewater treatment. But, if the applied voltage was higher than 5 V, it ultimately decreased the % T and % M because of the friction between the charges due to high voltage. The mineralization of the

Table 2 Statistical analysis of independent variables and its effect on the selected responses for hPEF treatment process

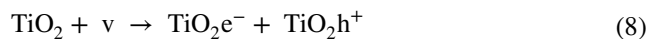
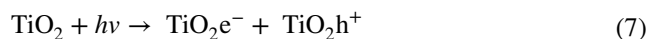
	% T					% M					EC					
	Estimate	Std. Error	t-value	Pr(> t)	Estimate	Std. Error	t-value	Pr(> t)	Estimate	Std. Error	t-value	Pr(> t)	Estimate	Std. Error	t-value	Pr(> t)
Intercept	75.38	3.11	5.3096	0.0001	65.38	3.61	6.8200	0.0001	1.05	0.0668	5.2194	0.0001	1.05	0.0668	5.2194	0.0001
pH	-14.37	1.55	-2.3094	0.0001	-14.87	1.80	-0.5511	0.0001	0.2126	0.0334	2.2702	0.0001	0.2126	0.0334	2.2702	0.0001
Time	1.25	1.55	1.5013	0.4340	2.08	1.80	1.3727	0.2667	0.4789	0.0334	1.4758	0.0001	0.4789	0.0334	1.4758	0.0001
Voltage	-0.4775	1.55	0.1055	0.7627	0.3558	1.80	1.2102	0.8463	0.1382	0.0334	0.1037	0.0009	0.1382	0.0334	0.1037	0.0009
Fe dose	-14.15	1.55	-0.6138	0.0001	-13.32	1.80	-2.0730	0.0001	-0.1440	0.0334	-0.6034	0.0006	-0.1440	0.0334	-0.6034	0.0006
pH X Time	3.67	1.90	0.3086	0.0725	2.42	2.21	0.0276	0.2900	0.0548	0.0409	0.3034	0.2006	0.0548	0.0409	0.3034	0.2006
pH X Voltage	5.90	1.90	0.6826	0.0073	4.65	2.21	0.8640	0.0526	0.0015	0.0409	1.1196	0.9720	0.0015	0.0409	1.1196	0.9720
pH X Fe dose	6.51	1.90	2.2051	0.0038	5.26	2.21	0.8509	0.0310	0.0504	0.0409	0.0125	0.2369	0.0504	0.0409	0.0125	0.2369
Time X Voltage	1.82	1.90	0.0533	0.3547	3.07	2.21	2.4726	0.1855	0.0233	0.0409	0.6686	0.5770	0.0233	0.0409	0.6686	0.5770
Time X Fe dose	-8.47	1.90	-0.7841	0.0005	-7.22	2.21	-1.2954	0.0052	-0.0715	0.0409	-1.5433	0.1012	-0.0715	0.0409	-1.5433	0.1012
Voltage X Fe dose	0.8225	1.90	0.7587	0.6716	2.07	2.21	0.4930	0.3632	0.0152	0.0409	4.2914	0.7154	0.0152	0.0409	4.2914	0.7154
pH ²	-12.90	1.45	-0.5608	0.0001	-12.28	1.69	-1.0395	0.0001	-0.0144	0.0313	-2.1042	0.6514	-0.0144	0.0313	-2.1042	0.6514
Time ²	0.1771	1.45	1.1389	0.9046	0.3021	1.69	0.5603	0.8603	-0.0044	0.0313	-1.7548	0.8897	-0.0044	0.0313	-1.7548	0.8897
Voltage ²	-10.69	1.45	-0.0127	0.0001	-10.56	1.69	-0.4581	0.0001	0.0087	0.0313	0.1370	0.7842	0.0087	0.0313	0.1370	0.7842
Fe dose ²	-2.18	1.45	-0.680	0.1534	-2.06	1.69	-0.4474	0.2413	-0.0582	0.0313	-0.4023	0.0825	-0.0582	0.0313	-0.4023	0.0825

Significance codes: 0 '***' 0.001 '**' 0.01 '*' 0.05 '.' 0.1 ' ' 1

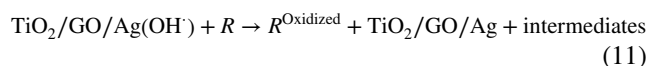
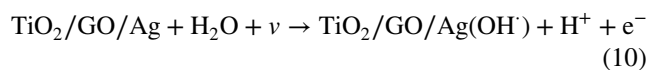
Table 3 ANOVA for the hPEF responses

	% T				% M				% EC				
	DF	Sum of square	Mean square	F-Value	Pr(>F)	Sum of square	Mean square	F-Value	Pr(>F)	Sum of square	Mean square	F-Value	Pr(>F)
Block.CCD	1	142.1	142.07	30.37	0.0001	206.6	206.56	0.4071	0.0001	1.2942	1.29418	5.3334	0.0001
FO (pH, Time, Voltage, Fe dose)	4	3577.2	894.29	19.118	0.0006	3659.6	914.89	1.8030	0.6052	0.6641	0.16604	0.6843	0.0001
TWI (pH, Time, Voltage, Fe dose)	6	4951.8	825.31	27.643	0.0016	5648.1	941.35	1.8552	0.0781	1.6589			
	0.27648	1.1394	0.9720										
PQ (pH, Time, Voltage, Fe dose)	4	1355.7	338.92	24.50	0.0001	1227.1	306.78	0.6046	0.0001	0.9367	0.23418	0.9651	0.0009
Residual	18	577.03	38.47			607.40	40.49			0.4020	0.0268		
Lack of Fit	10	348.64	34.86	0.7633	0.666	385.26	38.53	0.8672	0.6051	0.4020	0.0402	3.2062	
Pure Error	8	228.39	45.68			222.13	44.43			0.0000	0.0000		

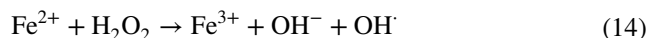
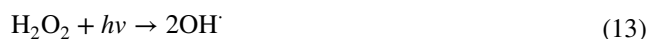
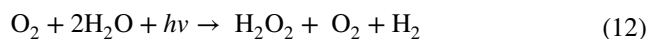
drug components was achieved by the synergic effect of the photo-Fenton and electro-Fenton processes. Moreover, under the synergic effect, there was the photocatalytic, voltage triggered, and electrochemical generation of OH• (Parrino et al. 2014). The photogenerated and voltage trigger electron in the conduction band of TiO₂ (Eqs. 7 and 8) and react with the oxygen to generate O₂•⁻ radicals (Eq. 9).



In the case of electro-Fenton, the OH• generated at the anode and then adsorbed on the anode surface as explained in Eq. (10), and the drug was mineralized through oxidation as explained in Eq. (11) (Santoke et al. 2009).



Besides, the hydroxyl radicals can be produced by ultraviolet irradiation of dissolved oxygen and action of Fenton reagent according to Eqs. (12–15) (Steter et al. 2014; Tilley 2019):



Hematite and goethite have a conduction band level at -0.62 and -0.08 V and a valence band level at +1.40 and +1.94 V, respectively. It has been observed that the excited electron (e⁻) of hematite conduction band would be easily transferred to the conduction band of goethite and an effective electron separation and transformation occur between the mixture of iron oxides (Tippmann 2015). Goethite has higher crystallinity and high photocatalytic activity. It supports the catalytic activity in weak acidic conditions by the formation of Fe₂(OH)₂⁴⁺ complex. It can be further photoreduced to hydroxyl radical and Fe²⁺ (Eq. 16):



It proclaimed that bupropion degradation was due to OH•⁻ mediated oxidation on the electrode and OH•⁻ and O₂•⁻-mediated oxidation attributed in the bulk.



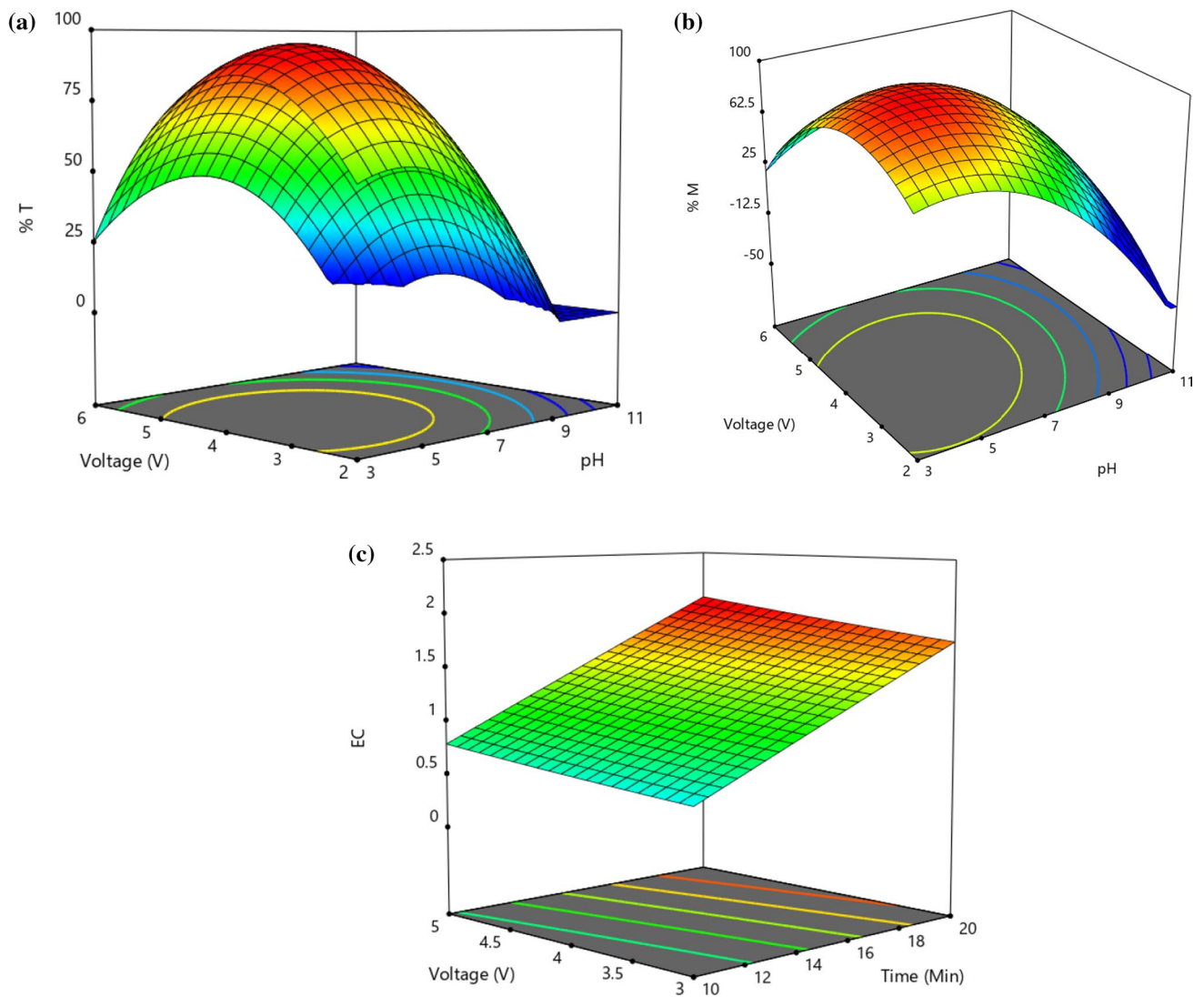


Fig. 2 Interaction of independent parameters with %T, %D, and EC

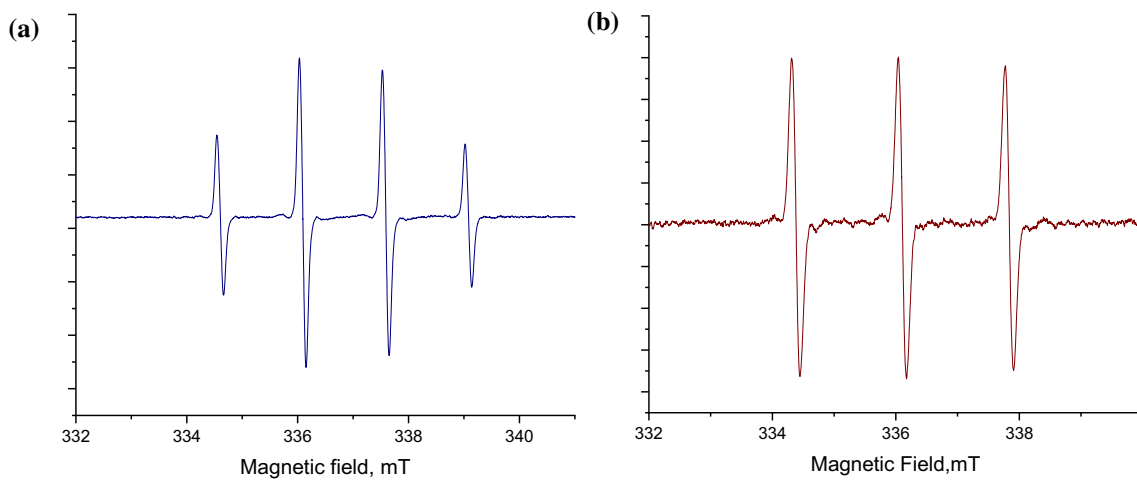


Fig. 3 Spin adducts of $\bullet\text{OH}$ and $\bullet\text{O}_2^-$ radicals observed by the EPR spectroscopy

To optimize the values of operating parameters, the target was set to maximize %*T* removal and %*M*, while keeping EC as a minimum. As a result, the optimum condition was found by desirability function approach using R programming: pH = 5.8, voltage = 3.6 V, time = 20 min, and Fe dose = 0.42 mM with predicted responses as: %*T* = 89.16%, %*M* = 97.64%, and EC = 1.39 Wh. A set of three experiments was conducted at optimized condition (pH = 5.8, *V* = 3.6v, *t* = 20 min, and Fe dose = 0.42 mM). The predicted responses and experimental values at the optimal conditions satisfy the suitability of optimization analysis, and the average values derived are: %*T* = 87.86%, %*M* = 97.09%, and EC = 1.35 Wh, which were in good agreement with the predicted values.

Degradation pathway and disinfection study

To study the degradation pathway, transformation products play an important role. To determine the transformation by products of bupropion hydrochloride, 10 ng L⁻¹ of drug solution was treated by hPEF at achieved optimize conditions for 20 min. This treatment was performed at a higher concentration of bupropion hydrochloride, to detect the reaction transformants accurately. Samples for the GC–MS analysis were withdrawn from the ongoing reaction at specific intervals of time. The mass spectrum obtained from GC–MS analysis for the initial sample (without hPEF treatment) shows a peak at 100 with a mass/charge (*m/z*) ratio (Fig. SI-3). The GC–MS mass spectrum of samples after hPEF treatment for 20 min (Fig. SI-3) divulged the formation of four considerable reaction intermediates. Bupropion hydrochloride-transformed products are listed in Table SI-3 according to their retention time.

During hPEF of bupropion hydrochloride wastewater, there were two oxidative species predominantly participating in the degradation process such as OH[•] and O₂^{•-}. This was confirmed by EPR spectroscopy. For EPR, 5,5'-dimethylpyrrolidine N-oxide (DMPO) and 2,2,6,6-tetramethylpiperidine 1-oxyl (TEMPO) were used for radicals trapping. The spin adducts observed by the EPR (DMPO) represent the presence of four distinctive peaks having an intensity proportion of 1:2:2:1 (Fig. 3a). It ensured the generation of OH[•] in the hPEF treatment process (Wang et al. 2017), while 2,2,6,6-tetramethylpiperidine 1-oxyl (TEMPO) showed a typical signal of three peaks with an intensity of 1:1:1. The signal intensity secured the presence of O₂^{•-} radicals as shown in Fig. 3b.

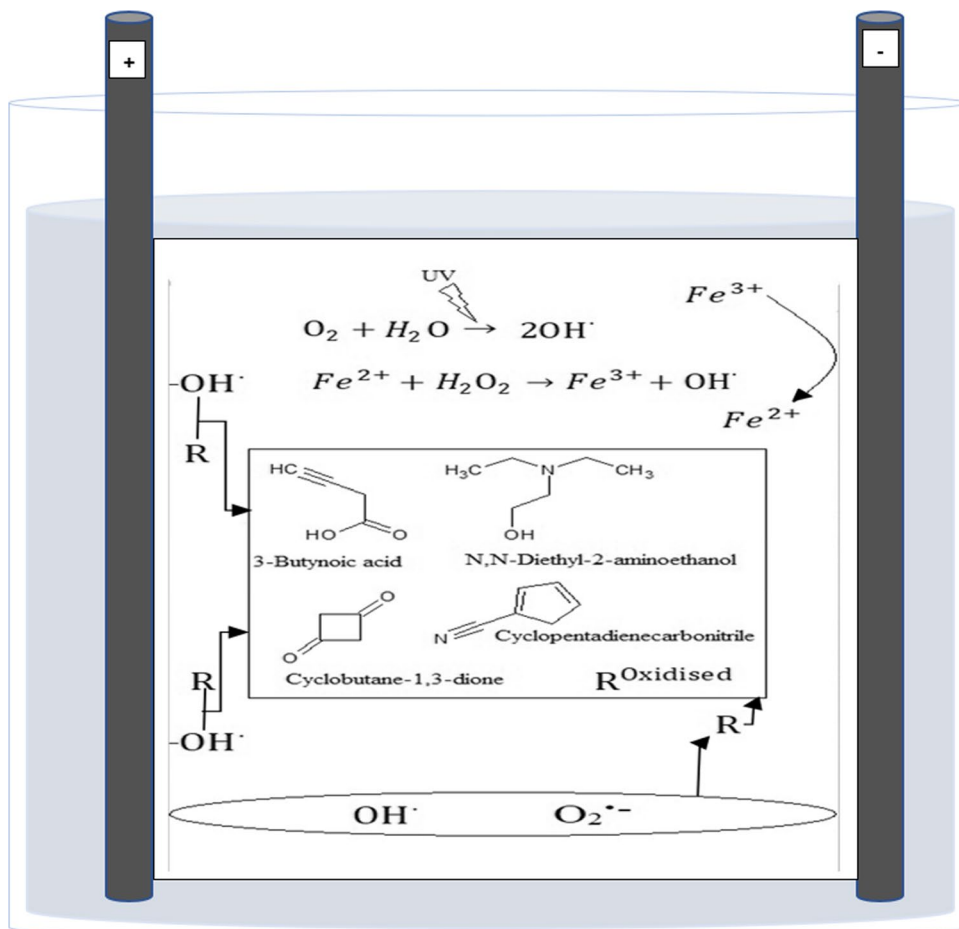
Degradation pathway has been predicted based on the generated transformants and involvement of OH[•] and O₂^{•-} radicals to degrade the bupropion hydrochloride molecule (Fig. 4). According to one possible pathway, (ipso attack) aromatic characteristics of bupropion molecules

would be shattered with the addition of the OH[•] radical (Xu et al. 2019). The direct attack of hydroxyl radicals would break the benzene ring by the dealkylation of the bupropion molecule. In this case, possibly N,N-diethyl-2-amino ethanol (*m/z* 117) and 3-butynoic acid or cyclobutene-1,3 dione (*m/z* 84) transformants would be formed. The breaking of the benzene ring promotes the generation of unstable alcohol and acid intermediates (Yang et al. 2013). In another degradation pathway, there is a possibility of an intermediate generation (cyclopentadiene carbonitrile with *m/z* 252.9) by decarboxylation due to the attack of active O₂[•] species. Complete dealkylation of cyclopentadiene carbonitrile would result in the complete mineralization. It was observed that the peak area of N, N-Diethyl-2-amino ethanol increased concerning an increase in reaction time. A small peak with *m/z* ratio 100 of bupropion was observed after 20 min of hPEF treatment (Fig SI-3). It was observed because TOC removal (90%) from bupropion-polluted wastewater through hPEF treatment was below 100%. Furthermore, generated transformants would undergo oxidation, be converted into aliphatic compounds, and then ultimately yield Cl₂, NO₂, CO₂, and H₂O. The dissociation of bupropion molecules was also observed by FTIR spectra.

The FTIR spectrum of before treatment (*t* = 0) and after treatment sample (*t* = 20 min) is shown in Fig SI-4a. Two prominent peaks were observed in the spectrum of before treatment sample at 3309.70 and 1633.73 cm⁻¹. These peaks were adsorption peaks of amine, hydroxyl functional, and carbonyl groups, respectively, present in the molecule of bupropion (Ye et al. 2019a). The adsorption intensity of these groups was reduced after hPEF treatment. There were small peaks generated at 1455, 1745, 2849, and 2923 cm⁻¹ after hPEF as shown in Fig SI-4a, which was characteristic adsorption peaks of H–C–H bend, –C=O, C–H, and C–H (weak stretch) groups. Therefore, the FTIR spectrum proves that the bupropion molecules were breakdown into transformants. These transformants undergo further oxidation and are converted into simpler compounds. It was also confirmed by the UV–visible spectra of initial and treated synthetic wastewater sample as shown in Fig SI-4b. An initial sample of bupropion simulated wastewater exhibited two maxima at 208 and 251 nm. However, these peaks significantly diminished in the spectrum of the treated sample by hPEF.

Bupropion wastewater containing *E. coli* culture was treated without UV-C, to determine the sole effect of Ag to disinfect the wastewater at the optimized condition. It was observed that after electrochemical treatment, the CFU count extensively reduced up to 40,000 CFU from 58,000 CFU. The *E. coli* cells viability was reduced up to 13.8% after electro-oxidation treatment (EO). After the (Ag + UV-C) hPEF treatment, it was decreased to 5015 CFU. It was

Fig. 4 Degradation pathway and generated transformants during hPEF treatment of bupropion hydrochloride



observed that Ag solely was effective for the disinfection of hPEF treated wastewater, but the combination of Ag and UV-C was extremely effective to disinfect the wastewater, and the viability of cells was reduced by 91.4% at optimized conditions. The presence of *E. coli* culture in the wastewater before treatment was observed under the microscope as shown in SI-5a and b. It was observed that the metabolic activity of the *E. coli* cells was reduced to 10% after electrochemical treatment and furthermore after (Ag + UV-C) hPEF treatment, it was reduced up to 89%. The cytotoxicity was high with (Ag + UV-C) hPEF treatment as shown in Fig. 5, but the survived *E. coli* cells have deformed cell wall or naked cells with the effect of UV-C radiation.

Degradation kinetics

Degradation kinetics was performed with pseudo-first-order, first-order, and second-order model. The pseudo-first-order model (Eq. 17) follows bupropion degradation from

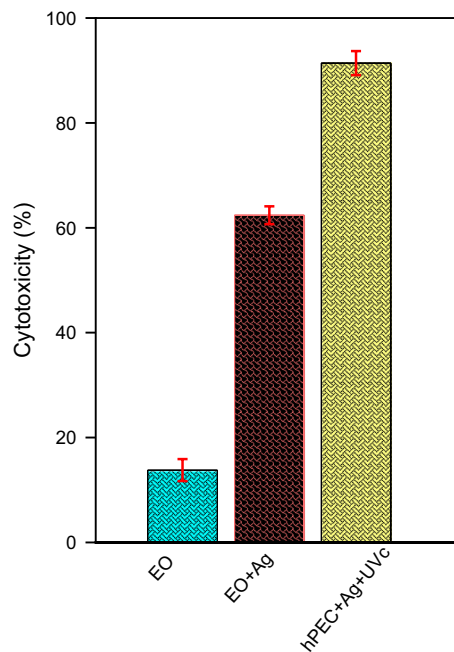


Fig. 5 Cytotoxicity of hPEF, Ag, and UV-C

simulated pharmaceutical wastewater by hPEF process at any time very well.

$$\ln \frac{C_0}{C_t} = kt \quad (17)$$

where C_0 is the initial concentration of bupropion organic carbon. At any instant value of C_t and applied voltage, the initial bupropion mineralization rate is high but as it attains equilibrium, a small fraction of initial bupropion organic carbon (C_0) was left unoxidized at the experimental conditions. Therefore, the pseudo-first-order model equation was modified for a better understanding of the kinetic model (Eq. 18) (Ye et al. 2019b).

$$C_{Mt} = C_{Me} [1 - e^{k_p t}] \quad (18)$$

where C_{Mt} (mgL^{-1}) is the concentration bupropion organic carbon at any instant of time (t), whereas C_{Me} (mgL^{-1}) is the concentrations of bupropion organic carbon mineralization at equilibrium condition and k_p is the reaction rate constant. A nonlinear kinetic study was performed at optimized conditions (voltage = 3.6 V, pH = 5.8 ± 0.1 , Fe dose = 0.42 mM) for the bupropion TOC concentration change concerning hPEF reaction time. Marquardt's percent standard deviation (MPSD) (Eq. 19) applying error function was used for the fitting of experimental data into the nonlinear regression (Zhu et al. 2016):

$$\text{MPSD} = 100 \sqrt{\frac{1}{m-n} \sum_{i=1}^n \frac{C_{Mt,v,\text{epm}} - C_{Mt,v,\text{calc}}}{C_{Mt,v,\text{exp}}}} \quad (19)$$

where the 'epm' and 'calc' symbolize the experimental and calculated values of total organic carbon, respectively, and m and n represent the number of measurements and parameters, respectively, in the model. Pseudo-first-order kinetic model was fitted to experimental data for the mineralization of bupropion removal as shown in Fig SI-6. The best-fitted parameters for the nonlinear kinetic model are shown in Table SI-4. It was observed that reaction equilibrium was achieved in 19 min for bupropion degradation. Consequently, degradation kinetics of bupropion was investigated within the time range of 30 min. Pseudo-first-order kinetic model was accurately fitted with high R^2 (0.99) value at the optimized conditions for bupropion degradation by hPEF. The correlation between the $C_{Me,\text{exp}}$ and $C_{Me,\text{calc}}$ values proves the accuracy of the pseudo-first-order kinetic model.

Conclusion

Hetero-photo-electro-Fenton is a versatile and robust method and suitable for the degradation of all types of wastewaters even operating at close to neutral pH range of 5–7. The combination of photo- and electrocatalysis using $\text{TiO}_2/\text{GO}/\text{Ag}$ -loaded electrode is very effective for the mineralization of bupropion drug. Hetero-photo-electrocatalysis was successfully performed in batch for bupropion-laden wastewater treatment. Statistical analysis advocates a high correlation between the observed and predicted values. Hetero-photo-electrocatalysis process was successfully optimized for important process parameters with Rcmdr (design) package by using the response surface central composite design (fractional factorial two-level design). It was confirmed that two oxidative species such as $\bullet\text{OH}$ and $\bullet^-\text{O}_2^-$ played an important role in the degradation of organics. The maximum TOC removal and mineralization at the optimum conditions by the hPEF treatment were found to be 87.86% and 97.09%, respectively. The mineralization kinetics follows pseudo-first-order kinetic for hPEF treatment process. hPEF, Ag, and UV-C in combination were found to be very effective for the disinfection of the wastewater as compared to electrochemical oxidation.

From an environmental point of view, the present study concentrates on energy consumption, safe disposal, and minimizing the iron (Fenton's catalyst) and electrocatalyst leaching in treated wastewater. To minimize the energy consumption, an approach was used to emerge photocatalysis and electrocatalysis, to reduce the degradation time, which ultimately minimize the energy consumption ($\text{EC} = 1.35 \text{ Wh}$). hPEF treatment energy was also used for the disinfection of wastewater by modifying the electrode material. It has been reported that graphene oxide has disinfection properties (Zickler et al. 2006) but in the presence of Ag and UV-C, it provided extremely good disinfection results. To make this process safer for the disposable point of view, goethite and hematite nanoparticles were used as Fenton's reagent. These help to protect the hydroxyl radicals at higher pH range and provide liberty to perform hPEF treatment of pharmaceutical wastewater at less acidic pH. To determine the iron leaching, iron concentration in the hPEF-treated wastewater was observed, which was 0.02 mg/l, revealing the fact that iron leaching is quite low as compared to the photo-Fenton process.

Supplementary Information The online version contains supplementary material available at <https://doi.org/10.1007/s13762-022-04065-3>.

Acknowledgements The authors would like to acknowledge the support provided by MVTT Foundation of Finland. This work was also supported by the Distinguished Scientist Fellowship Program (DSFP) at King Saud University, Riyadh, Saudi Arabia, and Ahmed A.S. Al-Othman (Department of Agricultural Engineering, College of Food Sciences and Agriculture, King Saud University, P.O. Box 2460, Riyadh 11451, Saudi Arabia).

Funding Open Access funding provided by Aalto University.

Open Access This article is licensed under a Creative Commons Attribution 4.0 International License, which permits use, sharing, adaptation, distribution and reproduction in any medium or format, as long as you give appropriate credit to the original author(s) and the source, provide a link to the Creative Commons licence, and indicate if changes were made. The images or other third party material in this article are included in the article's Creative Commons licence, unless indicated otherwise in a credit line to the material. If material is not included in the article's Creative Commons licence and your intended use is not permitted by statutory regulation or exceeds the permitted use, you will need to obtain permission directly from the copyright holder. To view a copy of this licence, visit <http://creativecommons.org/licenses/by/4.0/>.

References

- Aliofkhaezai M (2014) Modern electrochemical methods in nano, surface and corrosion science (Ed.), ISBN: 978-953-51-1586-1 <https://doi.org/10.5772/57202>
- An X, Tang Q, Lan H, Liu H, Qu J (2019) Polyoxometalates/TiO₂ fenton-like photocatalysts with rearranged oxygen vacancies for enhanced synergetic degradation. *Appl Catal B Environ* 244:407–413. <https://doi.org/10.1016/j.apcatb.2018.11.063>
- Cheng X, Liu H, Chen Q, Li J, Wang P (2014) Preparation of graphene film decorated TiO₂ anano-tube array photoelectrode and its enhanced visible light photocatalytic mechanism. *Carbon N Y* 66:450–458. <https://doi.org/10.1016/j.carbon.2013.09.021>
- Chèvre N (2014) Pharmaceuticals in surface waters: sources, behavior, ecological risk, and possible solutions case study of Lake Geneva, Switzerland. *Wiley Interdiscip Rev Water* 1(1):69–86. <https://doi.org/10.1002/wat2.1006>
- Farshchi M, Aghdasinia H, Khataee A (2019) Heterogeneous fenton reaction for elimination of acid yellow 36 in both fluidized-bed and stirred-tank reactors: computational fluid dynamics versus experiments. *Water Res* 151:203–214. <https://doi.org/10.1016/j.watres.2018.12.011>
- Fatta-Kassinos D, Meric S, Nikolaou A (2011) Pharmaceutical residues in environmental waters and wastewater: current state of knowledge and future research. *Anal Bioanal Chem* 399(1):251–275. <https://doi.org/10.1007/s00216-010-4300-9>
- Feng J, Hu X, Yue P (2006) Effect of initial solution Ph on the degradation of orange II using clay-based Fe nanocomposites as heterogeneous photo-fenton catalyst. *Water Res* 40(4):641–646. <https://doi.org/10.1016/j.watres.2005.12.021>
- Fox J, Andronic L, Ash M, Boye T, Calza S, Chang A, Lesnoff M (2012) Rcmdr: R Commander, R package version 1.6–3. *CRAN Rproject.org / package = Rcmdr* (March 2012). <http://socserv.socsci.mcmaster.ca/jfox/Misc/Rcmdr/>
- Gao B, Peng C, Chen GZ, Li Puma G (2008) Photo-electro-catalysis enhancement on carbon nanotubes/titanium dioxide (CNTs/TiO₂) composite prepared by a novel surfactant wrapping sol-gel method. *Appl Catal B Environ* 85(1–2):17–23. <https://doi.org/10.1016/j.apcatb.2008.06.027>
- Hu W, Peng C, Luo W, Lv M, Li X, Li D, Huang Q, Fan C (2010) Graphene-based antibacterial paper. *ACS Nano* 4(7):4317–4323. <https://doi.org/10.1021/nn101097v>
- Jia J, Li D, Wan J, Yu X (2016) Characterization and mechanism analysis of graphite/C-doped TiO₂ composite for enhanced photocatalytic performance. *J Ind Eng Chem* 33:162–169. <https://doi.org/10.1016/j.jiec.2015.09.030>
- Kumar KV, Porkodi K, Rocha F (2008) Isotherms and thermodynamics by linear and non-linear regression analysis for the sorption of methylene blue onto activated carbon: comparison of various error functions. *J Hazard Mater* 151(2–3):794–804. <https://doi.org/10.1016/j.jhazmat.2007.06.056>
- Lawson J (2014) Design and analysis of experiments with R. Chapman and Hall/CRC, London
- Li F, Li X, Liu C, Liu T (2007) Effect of alumina on photocatalytic activity of iron oxides for bisphenol A degradation. *J Hazard Mater* 149(1):199–207. <https://doi.org/10.1016/j.jhazmat.2007.03.069>
- Lin P, Shen J, Tang H, Lin Z, Jiang Y (2019) Enhanced photocatalytic H₂ evolution of ultrathin G-C₃N₄ nanosheets via surface shuttle redox. *J Alloys Compd*. <https://doi.org/10.1016/j.jallcom.2019.151918>
- Lucas MS, Peres JA (2009) Removal of COD from olive mill wastewater by fenton's reagent: kinetic study. *J Hazard Mater* 168(2–3):1253–1259. <https://doi.org/10.1016/j.jhazmat.2009.03.002>
- Metcalfe CD, Chu S, Judt C, Li H, Oakes KD, Servos MR, Andrews DM (2010) Antidepressants and their metabolites in municipal wastewater, and downstream exposure in an urban watershed. *Environ Toxicol Chem* 29(1):79–89. <https://doi.org/10.1002/etc.27>
- Mondal SK, Saha AK, Sinha A (2018) Removal of ciprofloxacin using modified advanced oxidation processes: kinetics, pathways and process optimization. *J Clean Prod* 171:1203–1214. <https://doi.org/10.1016/j.jclepro.2017.10.091>
- Navalon S, Alvaro M, Garcia H (2010) Heterogeneous fenton catalysts based on clays, silicas and zeolites. *Appl Catal B Environ* 99(1–2):1–26. <https://doi.org/10.1016/j.apcatb.2010.07.006>
- Nidheesh P, Olvera-Vargas H, Oturan N, Oturan M (2017) Heterogeneous electro-fenton process: principles and applications. *Electro-fenton process*. Springer, Singapore, pp 85–110
- Paramasivam I, Jha H, Liu N, Schmuki P (2012) A review of photocatalysis using self-organized TiO₂ nanotubes and other ordered oxide nanostructures. *Small* 8(20):3073–3103. <https://doi.org/10.1002/sml.201200564>
- Parrino F, Camera-Roda G, Loddo V, Palmisano G, Augugliaro V (2014) Combination of ozonation and photocatalysis for purification of aqueous effluents containing formic acid as probe pollutant and bromide ion. *Water Res* 50:189–199. <https://doi.org/10.1016/j.watres.2013.12.001>
- Santoke H, Song W, Cooper WJ, Greaves J, Miller GE (2009) Free-radical-induced oxidative and reductive degradation of fluoroquinolone pharmaceuticals: kinetic studies and degradation mechanism. *J Phys Chem A* 113(27):7846–7851. <https://doi.org/10.1021/jp9029453>
- Steter JR, Barros WRP, Lanza MRV, Motheo AJ (2014) Electrochemical and sonoelectrochemical processes applied to amaranth dye degradation. *Chemosphere* 117(1):200–207. <https://doi.org/10.1016/j.chemosphere.2014.06.058>
- Tilley SD (2019) Recent advances and emerging trends in photo-electrochemical solar energy conversion. *Adv Energy Mater* 9(2):1–13. <https://doi.org/10.1002/aenm.201802877>
- Tippmann S (2015) Programming tools: adventures with R. *Nature* 517(7532):109–110. <https://doi.org/10.1038/517109a>



- Wang M, Zhang L, Zhang G, Pang T, Zhang X, Cai D, Wu Z (2017) In situ degradation of antibiotic residues in medical intravenous infusion bottles using high energy electron beam irradiation. *Sci Rep* 7(January):1–8. <https://doi.org/10.1038/srep39928>
- Xu A, Brillas E, Han W, Wang L, Sirés I (2019) On the positive effect of UVC light during the removal of benzothiazoles by photoelectro-fenton with UVA light. *Appl Catal B Environ* 259(July):118127. <https://doi.org/10.1016/j.apcatb.2019.118127>
- Yang N, Liu Y, Wen H, Tang Z, Zhao H, Li Y, Wang D (2013) Photocatalytic properties of graphdiyne and graphene modified TiO₂: from theory to experiment. *ACS Nano* 7(2):1504–1512. <https://doi.org/10.1021/nm305288z>
- Ye Z, Guelfi DRV, Álvarez G, Alcaide F, Brillas E, Sirés I (2019a) Enhanced electrocatalytic production of H₂O₂ at co-based air-diffusion cathodes for the photoelectro-fenton treatment of bronopol. *Appl Catal B Environ* 247(January):191–199. <https://doi.org/10.1016/j.apcatb.2019.01.029>
- Ye Z, Brillas E, Centellas F, Cabot PL, Sirés I (2019b) Electro-fenton process at mild PH using Fe(III)-EDDS as soluble catalyst and carbon felt as cathode. *Appl Catal B Environ* 257(April):117907. <https://doi.org/10.1016/j.apcatb.2019.117907>
- Zhu L, Santiago-Schübel B, Xiao H, Hollert H, Kueppers S (2016) Electrochemical oxidation of fluoroquinolone antibiotics: mechanism, residual antibacterial activity and toxicity change. *Water Res* 102:52–62. <https://doi.org/10.1016/j.watres.2016.06.005>
- Zickler GA, Smarsly B, Gierlinger N, Peterlik H, Paris O (2006) A reconsideration of the relationship between the crystallite size *l*_a of carbons determined by X-ray diffraction and raman spectroscopy. *Carbon N Y* 44(15):3239–3246. <https://doi.org/10.1016/j.carbon.2006.06.029>

